CFD SIMULATION OF COMBUSTION CHARACTERISTICS AND RE-IGNITION SOURCES IN A VALVELESS PULSE COMBUSTOR

Said M. A. Ibrahim[1], Mohamed R. Taha[2], *Mahmoud N. Al-Qammash[1]

[1] Mechanical Engineering Department, Faculty of Engineering, Al-Azhar University, Cairo, Egypt

[2] Mechanical Power Engineering Department, Faculty of Engineering, Cairo University, Giza, Egypt

*Corresponding author's E-mail: rwanmg@gmail.com

ABSTRACT

Due to the complex mechanism of the combustion process in the pulse combustor, it is challenging to conduct experimental applications to investigate the sources of re-ignition. The paper presents a 3D numerical simulation study of the re-ignition mechanism in a Helmholtz-type valveless pulse combustor. The numerical simulation is conducted by involving the fundamental equations of Reynolds averaged Navier-Stokes. The turbulence-chemistry interaction scheme is implemented using the Eddy Dissipation Model and a propane-air mixture utilizing a two-step process. The CFD combustion model was used to predict the limit cycle of thermoacoustic instability in a laboratory-scale pulse combustor and was examined with experimental results to assess its validity. Our simulation study revealed there was a weak re-ignition source at the beginning of the combustion chamber, but it was extinct due to insufficient thermal energy. The main re-ignition source occurs when the high-temperature gas in the hot zone recirculates in Counter-rotating and pulls the flame to extend around the bluff body. The combustible air-fuel mixture instantly interacts with the bluff body's extended flame, causing self-ignite to the downstream mixture flow. The results confirm that the model CFD simulations are capable of accurately capturing the periodic re-ignition sources and scientifically proving the Rayleigh criteria.

CFD SIMULATION OF COMBUSTION CHARACTERISTICS AND RE-IGNITION SOURCES IN A VALVELESS PULSE COMBUSTOR

محاكاة عدديه لخصائص الاحتراق ومصادر إعادة الاشتعال في جهاز احتراق نبضى بدون صمام

سعيد محمد علي إبراهيم ١ ، محمد رشاد طه ٢ ، محمود نصر القماش ١

١ قسم الهندسة الميكانيكية، كلية الهندسة ، جامعة الأزهر ، القاهرة ، مصر

٢ قسم هندسة القوى الميكانيكية، كلية الهندسة ، جامعة القاهرة ، الجيزة ، مصر

البريد الإلكتروني للمؤلف الرئيسي: *rwanmg@gmail.com

الملخص:

تناولت هذه الورقة وضع نموذج جديد لمحاكاة عملية الاحتراق في موقد نبضى بدون صمام يعمل بوقود البروبان. يتم إجراء المحاكاة العددية باستخدام CFD اعتمادا على الاحتراق النبضى لنموذج اختبار عملي لالتقاط مصادر إعادة الاشعال في دورة الاحتراق. يتم التحكم في المحاكاة العددية باستخدام متوسط معادلات رينولدز نافير- ستوكس. تم تصميم مخطط التفاعل بين الاضطراب والكيمياء باستخدام نموذج تبديد الدوامه مع آلية تفاعل ثنائية. هنا نكتشف أن هناك مصدر ضعيف لإعادة الاشتعال في منطقة خلط المدخل ولكنه انقرض بسبب عدم كفاية الطاقة المحلية. في حين أن المصدر الرئيسي يكون بسبب اللهب الممتد حول الجسم خدعة مع وجود غازات إعادة التدوير الساخنة التي تواجه شحنه الخلط الجديدة من الهواء والوقود حينها يبدأ في إعادة إشعال الخليط واستدامه الاحتراق. يتم إجراء تجارب عمليه للتحقق من صحة نموذج CFD الذي تم إنشاؤه. وقارنت نتائج النموذج بالقيم التي تم الحصول عليها من النموذج التجريبي والتي أظهرت اتفاقا جيدا ليكون اداه لتحسين جهاز الاحتراق النبضى.

1. INTRODUCTION

Because of the growing demand for highly efficient combustion systems as a result of fossil fuel depletion and rising energy consumption, more studies have been performed to get more insight into the pulse combustion mechanism. Pulse combustion phenomena are periodic combustion processes caused by the excitation of the acoustic frequency modes of pulse combustors coupling with heat release, resulting in intermittent combustion processes. The combustion terminology is generally related to this field, which is mentioned as self-excited combustion oscillations, thermoacoustic instabilities, and combustion-driven oscillations [1]. There are many advantages of pulse combustion over conventional combustion including, but not limited, no or few moving parts, high combustion intensities, and low pollutant emissions [2, 3].

The heat transfer coefficient on the flue gas side of a pulse combustor of the Helmholtz type was significantly increased in the pulse combustion. This was attributed to being probably due to flue gas oscillations resulting in a reduction in the boundary layer inside the tube [2]. The pulsejet can be classified into three main types: Helmholtz, Schmidt, and Rijke tube, depending upon the combustor configuration and the oscillation characteristics. Additional divisions are according to the valve operation technique [3,4].

● Valveless pulsejet engine, which has no moving parts but contains aerodynamic valves. These pulsejets use their geometry to control the flow of exhaust and fresh inlet gases. Valveless pulsejets are of low cost, lightweight, powerful, and easy to operate, so they operate without the troublesome reed valves that need frequent replacement [5].

● Valved pulsejet engine, in which the combustion process is controlled by mechanical valves to control the injection of fresh charge of fuel and air. They force the hot gases to move outside the combustor through the tailpipe only and allow fresh air and more fuel to enter through the intake. The use of flapper valves in valve pulsejets limits the reliability and longevity of the engine.

Pulse combustion can be characterized as a pressure-gain device where the benefits of pulse combustion include enhanced heat release rates in the combustion chamber and increased heat transfer rates in the resonance tubes. Experimental research was carried out on the Argus As 014 pulsejet

engines that were used to power the infamous V-1 "buzz" bombs during World War II, which appear to be the most mass-produced pressure gain combustors to date [6].

Pulse combustion applications start from drying systems to propulsion devices. Due to their simplicity, pulsejets offer a good solution to the interest among the defense industry in pulsejet technology, for propelling small lightweight Unmanned Aerial Vehicles (UAV) [7]. The relatively low thermal efficiency of pulsejets has always been the major obstacle in their development [8].

The higher thrust-to-volume and thrust-to-weight ratios are beneficial to the propulsion system. The dimensions of the combustion chamber have a significant impact on the design of the valveless pulse system. From statistical analysis, the thrust is directly related to the volume of the combustion chamber. Pulse combustion devices can successfully run on conventional fuels such as natural gas, propane, liquefied petroleum gas, and methane [9]. The authors [10] observed that the pulsating form of exhaust was stable and self-sustaining as long as the fuel was supplied in the design and development of the valveless pulsejet engine to operate with liquefied petroleum gas.

The ignition process mechanism in a Helmholtz-type valveless self-excited pulse combustor was investigated for the periodic re-ignition by conducting experiments using a high-speed camera to record the formation and variation of flame during the ignition process [11]. However, they did not specify the location of the ignition process mechanism in the pulse combustion. One of the early attempts to model the Helmholtz-type pulse combustor with self-sustained acoustic oscillation using CFD software was carried out by Benelli et al. [12]. The combustion dynamics of the pulse combustor were simulated numerically using CFD of a Large-Eddy Simulation (LES) [13]. The swirl not only helps to enhance better mixing of fuel and oxidants but also to promotes flame stability. The flame shape is one of the most critical and intuitive characteristics of combustion. Researchers studied the flame dimensions and pollutant emissions of high-pressure non-premixed swirl combustion [14].

The Pulse combustion characteristics for a variety of gaseous fuels are investigated by CFD. The CFD model for a mechanically-valved Helmholtz type pulse combustor was developed to simulate the essential dynamics of the flame structure and remark that the hot remnant gases from the previous cycle ignited the fresh fuel-air mixture without providing details [15]. The pulsating flow in the elbow tailpipe of a valveless self-excited Helmholtz pulse combustor is investigated numerically by FLUENT. Where the experimental measurements were concerned with pressures along the tailpipe and the internal and external elbow sections [15], the simulations show that: (1) the mean velocity decreases with the velocity amplitude along the tailpipe; (2) the mean and amplitude of area-averaged pressure for internal and external elbow pressures decrease along the tailpipe; and (3) the mean and amplitude of the internal elbow pressure are less than those of the external elbow. These agreed well with experiments. The mass-averaged velocity-reversing, formation of Dean vortices has contributed to an enhancement in convective heat transfer [16]. The researchers investigated the dynamic behavior of pulse combustors and analyzed the effect of different parameters on combustion stability, both theoretically and experimentally [17]. Authors [17] used a CFD model with forced mass flow at the inlet with a specified frequency to discuss the re-ignition sources in pulse combustion and found they may be attributed to three sources: the hot remnant gas near the inlet valve, the high-temperature chamber wall, and the unburned mixture where the other parameter effects are not shown.

This research is intended to study the combustion characteristics and re-ignition source mechanism that sustain continuous pulse combustion in a valveless pulse combustor. The simulation of realistic operating conditions and atmospheric pressure at the inlet is used to obtain the acoustic frequency of the pulse combustor, which contributes to improving our understanding and more insight into pulse combustion.

Particular focus is provided on the model simulation of the 3-dimensional pulse combustor that was created in the CFD software. Due to its simple geometry, a pulse combustor of the valveless type was typically designed and constructed for the present work. Propane is used as a fuel because of its portability, high energy and clean burning. The theoretical results from our developed model were accurately compared with the results of experiments used to verify and validate it.

2. THE NUMERICAL MODEL AND SOLUTION TECHNIQUES

Computational Fluid Dynamics (CFD) simulations are a very important tool for various combustion applications. CFD simulations are carried out in three key steps: the first is the geometry definition; the second is generating the mesh; and the third and most important step is the numerical solution of the flow domain. There are several methods for turbulent modelling in CFD simulations. One is the Reynolds Averaged Navier-Stokes (RANS), which is used in the present combustion simulation model in conjunction with the EDM, which is widely used in predictions of industrial combustion, with the (k-ε) turbulent model, while the P-1 uses a radiation model. The solution is divided into two stages: the first is a steady-state simulation, and the second is a transient simulation until the limit cycle is achieved with stable oscillation.

2.1. Governing Equations

The numerical study of the pulse combustion process requires extending the set of Navier-Stokes (NS) equations to include continuity, momentum, energy, species concentration equation, turbulence, and combustion equations. The turbulent flow is modeled with the k-ε turbulence model, as it is the most widely used and is valid for a wide variety range of flows. Because of its fast computational speed and ability to generate good results for diffusion flames, the EDM is one of the most commonly used combustion models. Hence the turbulence-chemistry interactions are based on the EDM which was developed by Magnussen-Hjertager in 1976. The EDM model is based on the notion that for both premixed and diffusion combustion, the overall reaction rate is controlled by the flow turbulence. The Numerical solution by the CFD model is applied to simulate the combustion instability in the flow field for the pulse combustor. The equations of continuity, momentum, energy, species transport, turbulence, and combustion equations are presented in what follows

Mass conservation equation

$$\frac{\partial \rho}{\partial T} + \frac{\partial \rho u_i}{\partial xi} = 0 \tag{1}$$

Species transport equation

$$\frac{\partial}{\partial T}(pY_k) + \frac{\partial}{\partial x_j}(pu_jY_k) = \frac{\partial}{\partial x_j}\left(pD_k \frac{\partial Y_k}{\partial x_j}\right) + \dot{\omega} + S_{Y_k}^S \tag{2}$$

Momentum equation

$$\frac{\partial \rho u_i}{\partial T} + \frac{\partial}{\partial xj}\left(\rho u_i u_j + p\delta_{ij} - \tau_{ij}\right) = 0 \tag{3}$$

Energy equation

$$\frac{\partial \rho E}{\partial T} + \frac{\partial}{\partial xi}\left[(\rho E + p)u_i + q_i - u_j\tau_{ij}\right] = 0 \tag{4}$$

Where: ρ is the mass density, p is the pressure, u_i is the velocity vector, and q_i is the heat flux vector.

The total energy per unit mass E is given by

$$E = e + \frac{1}{2}(u_k u_k) \tag{5}$$

The viscous stress tensor τ_{ij} is defined as

$$\tau_{ij} = \mu\left(\frac{\partial u_i}{\partial xj} + \frac{\partial u_j}{\partial xi}\right) - \frac{2}{3}\frac{\partial u_k}{\partial x_k}\delta_{ij} \qquad (6)$$

Where: e is the internal energy per unit mass and is computed by

$$e = h - \frac{p}{\rho} \qquad (7)$$

A two-step propane-air reaction mechanism is rapid equilibrium assumed in the combustion model, which is predefined in the FLUENT materials database, containing six species (C_3H_8, O_2, CO, CO_2, H_2O, and N_2) with the dissociation equation added.

$$C_3H_8 + 3.5O_2 \rightarrow 3CO + 4H_2O, and \qquad (8)$$

$$C + 0.5O_2 \rightarrow CO_2 \qquad (9)$$

Because of the high temperature in the combustion region, CO_2 dissociation occurs as

$$CO_2 \rightarrow CO + 0.5O_2 \qquad (10)$$

2.2. CFD Mesh Generating

Meshing is an integral part of the simulation process. Grid generation is a time-consuming activity that is a significant issue for the CFD analysis. ANSYS mesh is used to generate a mesh of the model by meshing tools within the ANSYS workbench. The geometrical discretization of the entire flow was called mesh or grid and it is composed of cells or elements, which are the control volumes. The mesh influences the accuracy, convergence, and speed of the simulation process. The computational mesh used in the present study is the three-dimensional one-eighth sector model with a grid element size of 2 mm and reduced to 1 mm in the inlet of air and fuel with a type of non-structured mesh. The grid of the computational domain is depicted in Figure 1. The grid quality is critical for the effectiveness of the CFD analysis, so the five inflation layers along the wall boundary and around the flame holder are used. All of the processes necessary to produce a mesh that can be read by the solver were addressed [18].
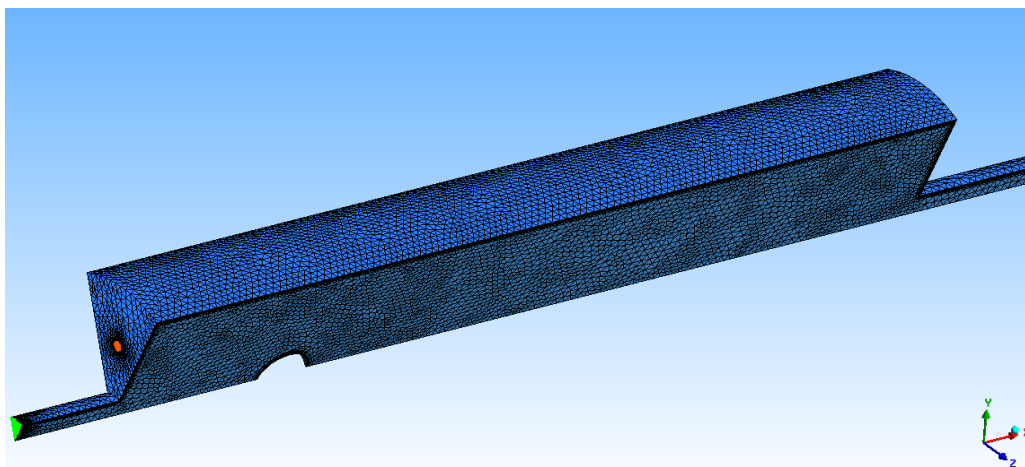

Figure 1. Mesh structure of the simulated 3D pulse combustor

2.3. Mesh Independence

A grid independent study is performed to get assurance that the numerical results are accurate and reliable with independent mesh size. Coarse mesh will result in inaccurate results, while high computational cost fine mesh will give better results compared to coarse mesh. It's significant important to get an optimal size that reaches a reasonable degree of precision and computational cost. Three different mesh set up is presented in **Table 1**. The pressure wave results obtained in the combustion chamber from three different meshes were compared through the model. As illustrated in Figure 2 the pressure profiles obtained at the chamber centerline, it can be noted that the two finer meshes have a good agreement according to their coincident. To reduce the computational cost and time-consuming in transient simulations, a middle-size mesh density has been employed and the solution would not be influenced by the choice of this mesh.

Table 1 Mesh Independence.

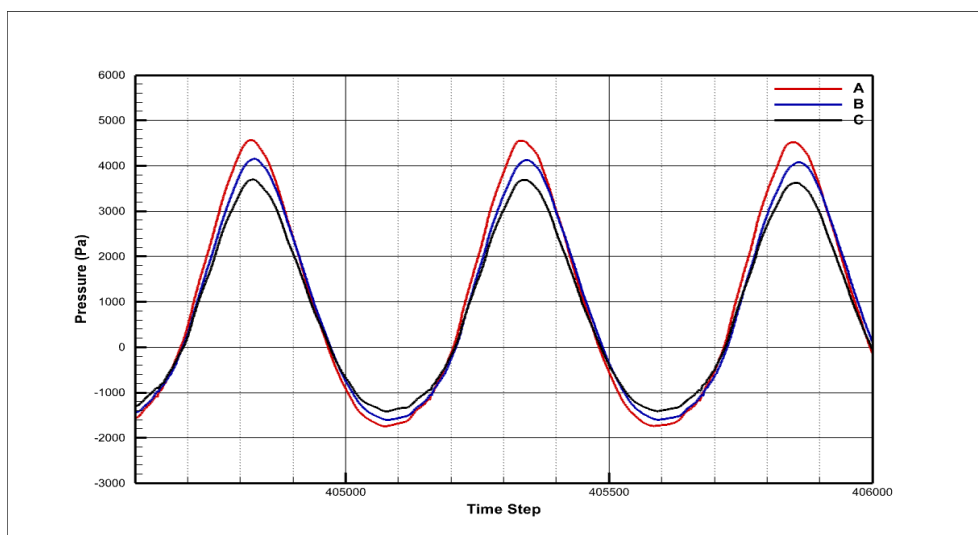| Mesh structure	A	B	C
Number of nodes	34251	43556	51547
Number of elements	107547	145657	173617

Figure 2. Comparison of the predicted local pressure variation for 3 different mesh

2.4. Solution Steps

Because the solution to this problem is very time-consuming, therefore we divided the solution into four steps. The first is to solve the steady-state conditions, the second is to use the steady-state solution from step one as initial conditions for the following unsteady state. This reduced the computation time significantly. The RANS solved the problem by using forced oscillation as internal exiting for triggering the mechanism at the inlet, and the atmospheric gauge pressure was applied at the outlet to create a pressure gradient, to initiate a fluid flow through the combustor to reach convergence. The third step is to use constant pressure at the inlet and solve the unsteady flow by using forced pressure disturbance at the outlet for a short duration of time to get a turbulent flow inside the combustor. In the fourth step, the inlet pressure is increased gradually and maintains atmospheric pressure at the outlet for thousands of time steps until pressure and temperature oscillations appear regularly, and fluctuate to reach the limit cycle.

2.5. Boundary and Initial Conditions

The boundary conditions adopted in this model are set as follows. The specific heat of each component is calculated using mixing law, while both thermal conductivity and viscosity are calculated by the ideal gas mixing law. The density is calculated by the ideal gas low. The thermal conductivity and viscosity of gas mixture are calculated by the ideal gas mixing law, and the constant dilute approximation is selected for the mass diffusivity calculation of the mixture. The symmetry boundary condition was applied to the calculation domain surface. The specified time step was set to be $1*10^{-5}$ s. The inlet propane and air mass flows are due to the sinusoidal pressure variation at the inlet port. At the exit of the tailpipe, atmospheric pressure and ambient temperature are specified. Non-slip solid wall conditions are assumed. The wall surface temperature is specified to convective and radiation heat transfer. The inlet propane-air mixture temperature is considered as 300 K, and stoichiometric mixture fraction for propane as fuel and O_2 as an oxidizer. The combustion is modeled as a two-step chemical reaction involving six species as specified in equations (8, 9). All equations are discretized by a second-order upwind scheme. The residuals of the model solution for continuity, momentum, species, and energy are set as program defaults for the convergence criterion.

2.6. Numerical Solution Procedures

The present CFD numerical model employs a segregated solution algorithm with a control volume-based method. The Semi-Implicit Method for Pressure-Linked Equations 'SIMPLE' algorithm uses a guess and correct procedure for the calculation of pressure on the staggered grid arrangement. It is used to couple the pressure and velocity for steady-state calculations. For transient calculations, the Pressure Implicit Solution by Split Operator 'PISO' method is adopted. EDM is used for the turbulent-chemistry interaction combustion model. The combustion temperature will rise above the practical value. That's because the EDM does not account for the dissociation of combustion products. By raising the specific heat of the combustion products, the Wang model corrects this issue [19]. The model setup was effective in triggering self-sustained pressure oscillations in the pulse combustor model geometry, meaning that the boundary conditions and parameters are appropriately chosen. Convergence of the discretized equations was defined as when the total field residual for all variables went below 10^{-3} for velocity and pressure, while the residual level for energy was maintained at 10^{-6}.

3. THE EXPERIMENTAL TEST RIG

The present model is used to simulate a valveless pulse combustor with the non-premixed inlet of propane and air. Figure 3 represents the real pulse combustor geometry. It consists of an air inlet pipe of 25 mm diameter and 50 mm length, fuel inlet holes alongside the surface of the combustion chamber with 4 mm diameter each. The total length and diameter of the combustion chamber are 280 and 75 mm, respectively, with a 20 mm diameter flame holder located at the end of the first quarter length of the combustion chamber. The tailpipe diameter is 20 mm and 1000 mm in length. Table 2 exhibits the geometrical dimensions of the pulse combustor. The main measured parameters are the propane fuel flow rate, which is measured using a flow rotameter, and the transient pressure oscillations measured by a piezoelectric transducer, with an amplifier and oscilloscope to display the results.

Table 2 Dimensions of the Pulse Combustor.

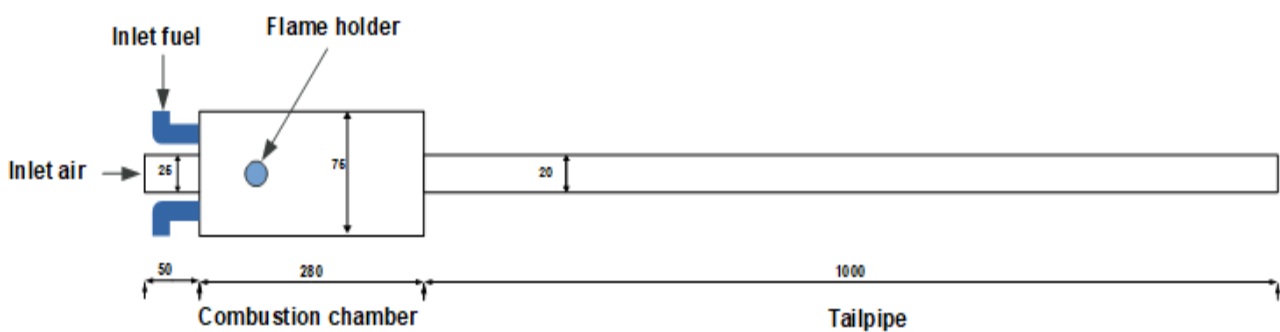| Values / Item	Diameter, m	Length, m	Area, m^2	Volume, m^3
Combustion chamber	0.075	0.28	0.0044	0.00124
Tailpipe	0.02	1	0.00031	0.00031
Inlet pipe	0.025	0.05	0.0000491	0.000025
Total pulse combustor				0.0015757

Figure 3. Pulse combustor test rig (dimensions in mm).

4. RESULTS AND DISCUSSION

4.1. Re-ignition Cycle Analysis

This section exhibits the results of the simulation of the combustion cycle along with appropriate explanations. Figure 4 shows the temperature and pressure contours plotted on the plane that crosses the center of the pulse combustor within the combustion chamber throughout one cycle to demonstrate the formation of the flame and the change in its structure. The stages of the present combustion cycle are:

● Combustion and exhaust

After air and fuel are introduced into the combustion chamber due to vacuum pressure at the inlet. The air and fuel mixes and react to commence the combustion in the pulse combustor. The generated high pressure caused by the combustion process results in the flame and hot product gases expanding through the combustion chamber. As shown in frame 1.013 s, the flue gases start to exit from the pulse combustor inlet and outlet gradually at high temperatures and velocity.

● Admission of air and fuel

Separate flow admission of air and fuel occurs into the pulse combustor through the inlet ports. The pressure drop after combustion and exhaust events is caused by flow inertia generated by flue gases exit at high velocity (kadenacy effect) as well as thermal shrinkage due to heat loss through the walls. The pressure decreases below the ambient pressure, as shown in frame 0.0139 s. The pulse combustor gradually draws new air while concurrently admitting propane fuel into the combustion chamber as the pressure falls until it reaches a minimum value lower than atmospheric pressure, as seen in frame 1.015 s.

● Compression

Fresh air and propane fuel continue to enter into the pulse combustor as long as the pressure in the combustion chamber is below the ambient condition. At the same time, reverse flow occurs in the exit pipe, which leads to compressing the incoming flow. Then the pressure starts to rise gradually within the combustion chamber, as shown in frame time 1.0169 s.

● Re-ignition

During the intake process, an early flame kernel is generated in the thin mixing layer before the flame holder, where the initiation of a very weak ignition occurs. The early flame kernel does not propagate with time due to insufficient associated energy to sustain its existence, and it is finally prone to extinction as shown in frame time 1.0158 s.

The outer recirculation zone and recirculation zones generated in the wake behind the flame holder are identified inside the combustion chamber by the velocity vector, as shown in the following right frames of Figure 4.

During the combustion and exhaust phases, the flame formation and propagates against the incoming flow due to the recirculation zones of hot gases produced behind the flame holder. Because the flame stretches around the flame holder in the direction opposite to the new charge of air and fuel, resulting in the generation of a new flame kernel associated with high energy. This was the main source of the re-igniting of the flammable mixture of gases within the hot mixing zone to form a flame initiation as is seen in frame 1.0169 s.

Due to enough thermal energy resulting from intense mixing of a hot product, flame growth and propagation around the flame holder can be seen in frames 1.0175 and 1.0183 s. As shown in frames 1.0183 -1.0196 s, the maximum heat release is coupled with the peak pressure, thus the flame with maximum temperature and peak pressure spreads downstream to the bulk flow again. These heat release rate oscillations drive instabilities when they are in phase with pressure oscillations. High pressure and temperature result in making the pressure wave travel through the pulse combustor to expand the product downstream to the tailpipe outlet and upstream through the inlet pipe, as seen in frames 1.0196 -1.021 s. Most of the flue gases exit from the combustion chamber, but the rest that remains in the combustion chamber and the tailpipe begin to cool down due to the heat loss through the wall surface to the surroundings. Meanwhile, a new charge of air and fuel is introduced into the pulse combustor at 1.025 s, and the cycle repeats itself. The combustion cycle indicates that the flame holder is a critical part of the combustion chamber that increases the turbulence and recirculation intensity, which results in enhanced mixing of hot gases and flame stability in the flame zone.

In the present model, the air-to-fuel ratio was 16:1. The relationship between the temperature contour and instantaneous contour lines plots of air-fuel equivalence ratio (the ratio of the actual air-fuel ratio to the stoichiometric air-fuel ratio)along with the combustion chamber during one cycle is exhibited in Figure 5.

Pressure oscillations in the combustor alter the fuel and airflow rates, which result in changes in the air-to-fuel mixture equivalence ratio. Inside the combustion chamber, the role of the mixture equivalence ratio fluctuation leads to the flame periodic fluctuation, creating heat release rate oscillations that result in thermo-acoustic instabilities. The wide range of the equivalence ratio fluctuations was found to vary significantly throughout the combustion cycle in the combustion chamber due to the non-premixed inlet method. Due to the temperature is a function of equivalence ratio, the air-fuel mixture can significantly vary, which influences the temperature distribution inside the combustion chamber.
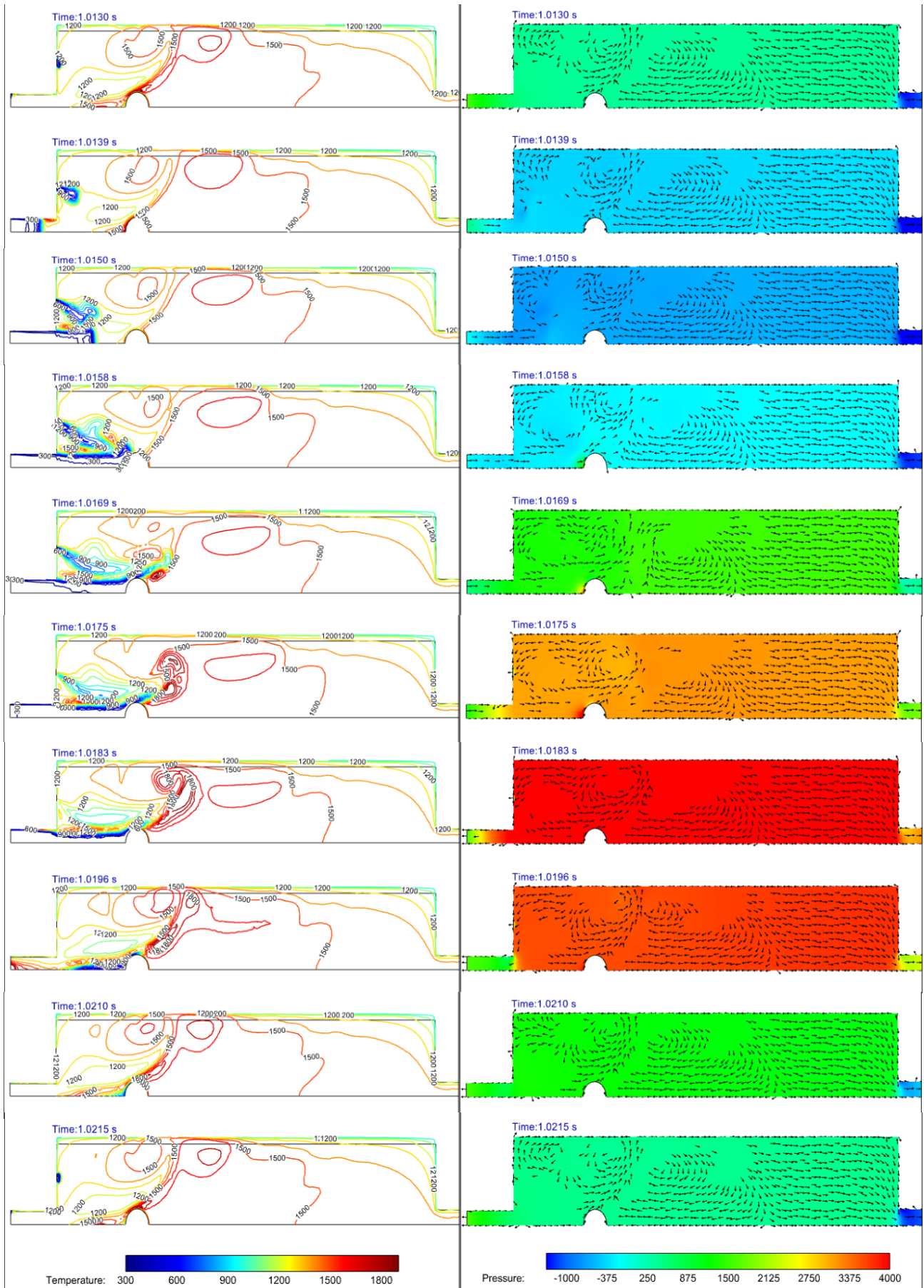
Figure 4. Evolution with time of the temperature and pressure through one cycle within the combustion chamber.

The mixture equivalent ratio contour lines change throughout the combustion chamber, from extremely lean near the air input due to continuous admission and exit of air, too rich near the flame holder due to unburned fuel through the cycle. According to Figure 5, the commencement of re-ignition happens around the value of unity (stoichiometric mixture) of equivalence air-fuel ratio at frame time 1.0169 s where the new kernel location is in a nearly stoichiometric region. The highest temperatures are located in the regions in front of the flam holder, ranging from the stoichiometric to the slightly rich mixture of equivalence ratios where the oxygen is consumed entirely at the frame of 1.0183 s. The flame temperature has significantly decreased with a reduction in equivalence air-fuel ratio contour lines as seen in Figure 5, frame 1.0196 s. A small amount of oxygen is left behind the flame holder during the combustion and subsequently consumed in the returned flame where the flame moves in the opposite direction, upstream into the inlet in the region of low velocity to re-ignite the new charge as exhibited in the frame time 1.0196 s.

The main products of propane combustion are CO_2 and CO, are shown in Figure 6, which illustrates the distribution of contours plotted for CO_2 on the left and CO on the right side of this figure. The imaging of two-dimensional simulations for CO and CO_2 distributions exhibits the mass fraction evolution during the pulse combustion cycle along the plane at the center of the combustion chamber within the pulse combustor model. The number of generating images, from simulation demonstrates the details of the combustion reaction progress with a two-step reaction model as in equations (8) and (9).

CO and CO_2 are produced as the reaction products due to the fuel being oxidized using the two-step reaction mechanism with rapid energy release. The largest heat release around the flame holder was predicted by the model through the maximum values of CO and CO_2 contours due to flame anchoring by the flame holder. The CO_2 produced in the flame diffuses into the recirculation zones with their associated high temperature.

Due to the recirculation in the wake region with the returned flame, the brightening red color of CO_2 around the flame holder boundary indicates the kernel is formed around the flame holder, whereas CO is released in frames 1.0159-1.0183 s. Because of the high residence time of the combustible mixture by recirculation, the re-ignition occurs at the location around the flame holder. The CO_2 reaches its maximum value when the mixture fraction at this time is stoichiometric and then reduces due to the decrease in oxygen concentration just after the start of combustion. After the combustion is completed, the values of CO_2 mass fraction emission have a constant value just after leaving the combustion zone and the tailpipe, which demonstrates that flue gases consist mainly of CO_2.

Since CO is an intermediate product of the hydrocarbon combustion process, its formation starts as soon as the reaction is initiated. As illustrated on the right frames of Figure 6, the flame initiation and propagation resulted in the appearance of CO rising upward around the flame holder along a part of it due to temperature increased of ignition in this region, where CO can be used to indicate the degree of radical formation. The CO into CO_2 conversion reactions is sensitive to temperature and oxygen availability in the pulse combustor. A weak evolution of CO concentration was observed on a series of right frames of Figure 6, due to high temperatures in the combustion which is used to oxidize CO into CO_2, which is one of the features of pulse combustion.
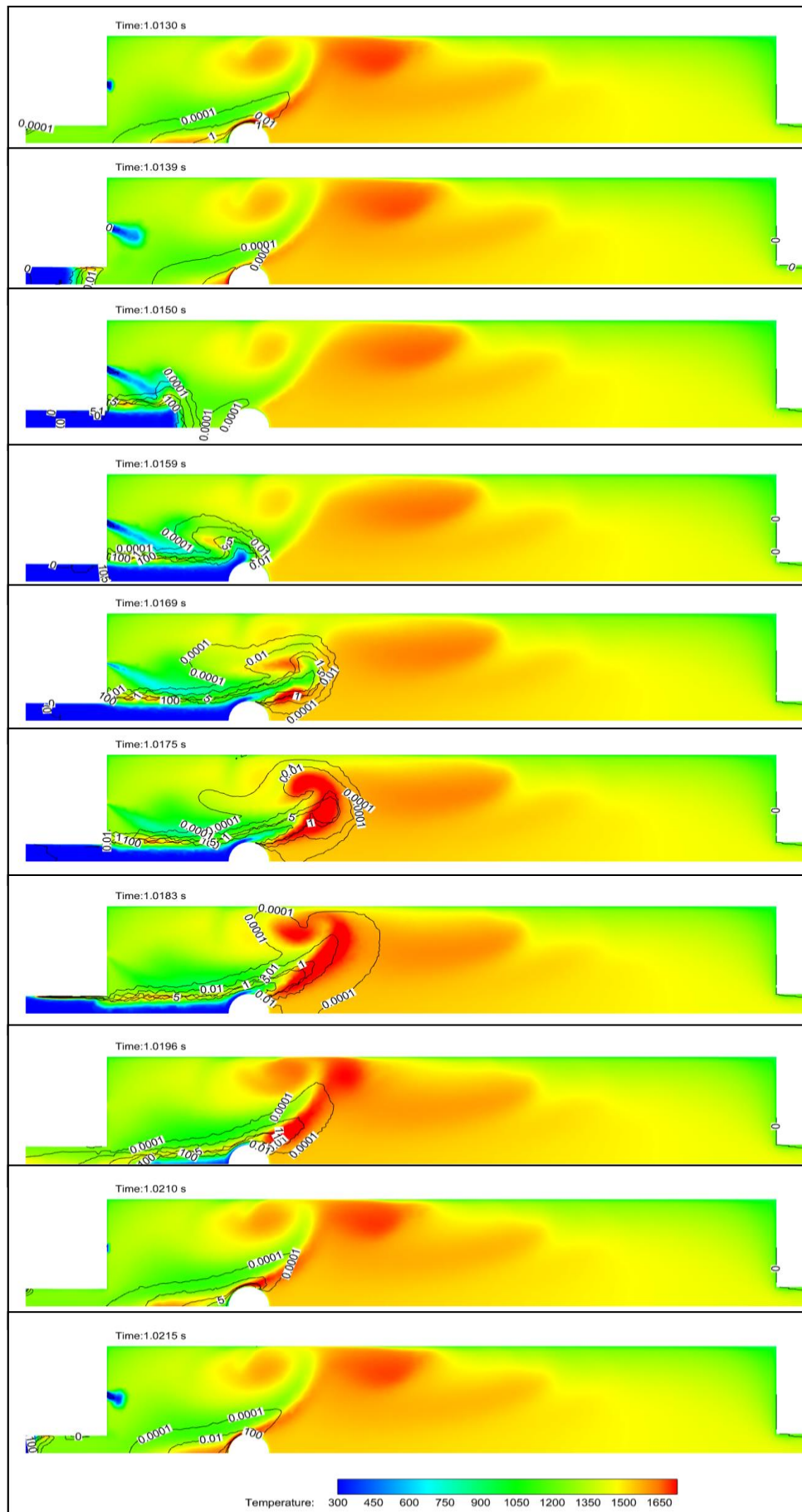
Figure 5. Evolution with time of the temperature distribution with equivalence ratio contour lines inside the combustion chamber.
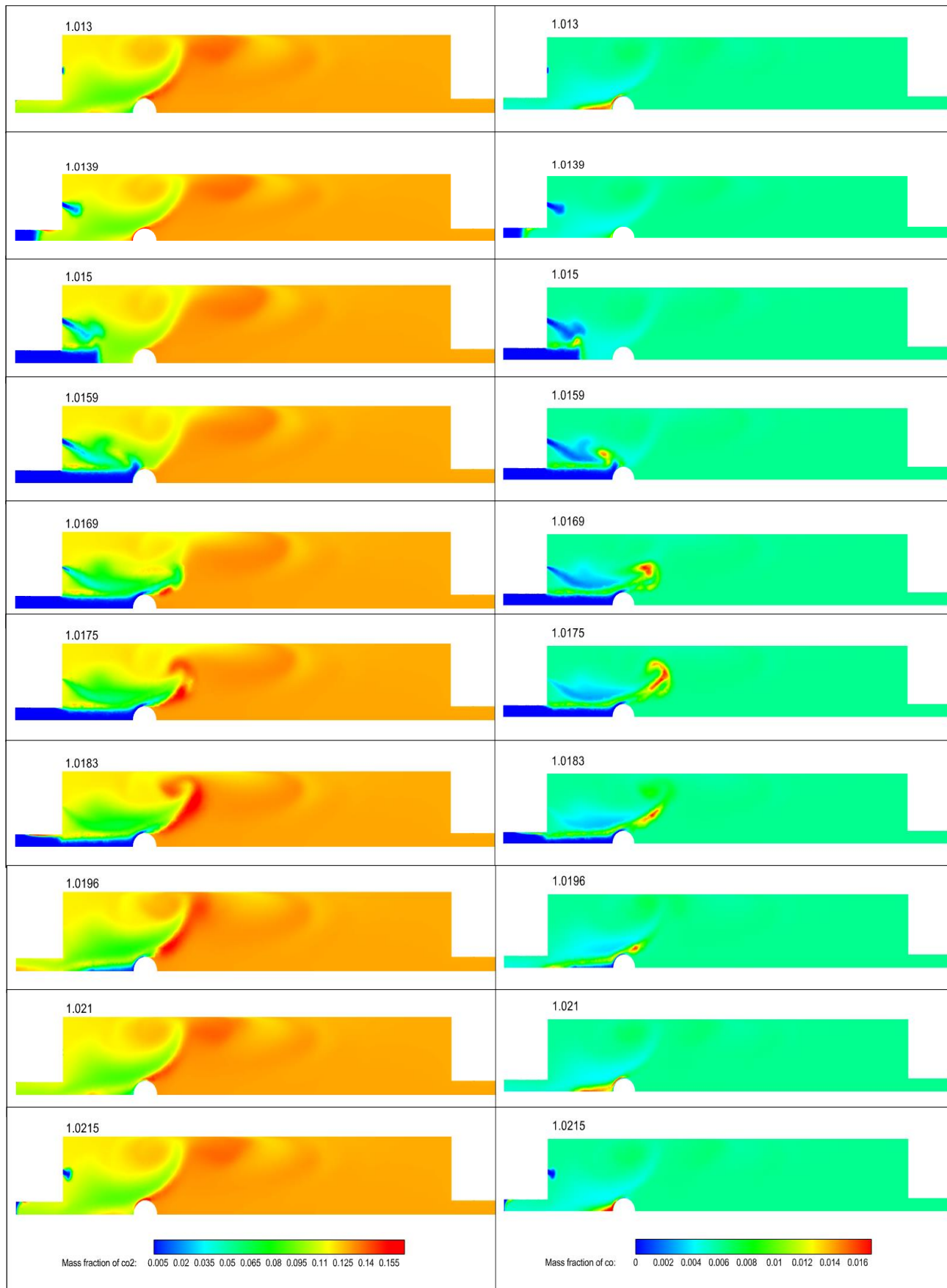
Figure 6. The evolution of CO₂ and CO mass fraction through one cycle, along with the combustion chamber.

4.2. Pulse Combustor Instability Analysis

The interaction of the combustion process with flow oscillations within the pulse combustor leads to combustion instability, which is a dynamic behavior. A closed feedback loop is created between the combustion process and flow oscillations, resulting in self-sustaining oscillations in which heat release and acoustic oscillations are in a phase relationship as depicted in Figure 7.
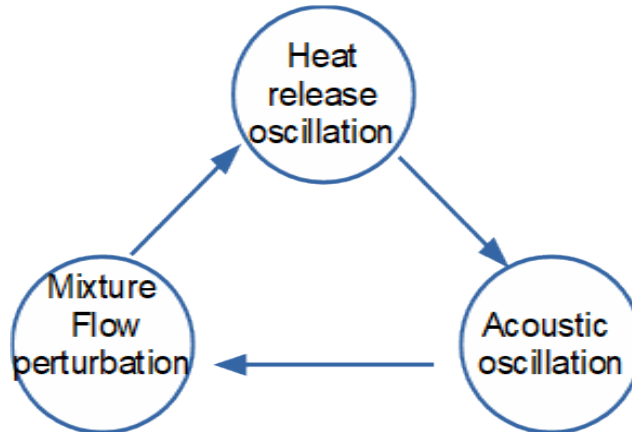
Figure 7. Feedback loop of combustion oscillations

The model simulation must be run multiple times initiated by low-pressure disturbances in the initial condition of the flow domain to produce the thermo-acoustic instability model and get pressure variations in the pulse combustor. The generated pressure fluctuation begins with exponential growth over time until it becomes regular with constant pressure amplitude after a long time, which is known as the limit cycle pressure oscillations

Figure 8 illustrates the operating state of pressure and temperature fluctuations from instability growth until the limit cycle operation state. It is worth noting that after running the model for a long time, it was found that the pressure amplitude increased in return to increasing the maximum degree of temperature until a balance was reached between heat release and wall heat loss. Finally, the amplitudes approach and achieve saturation, resulting in the occurrence of the limit cycle.
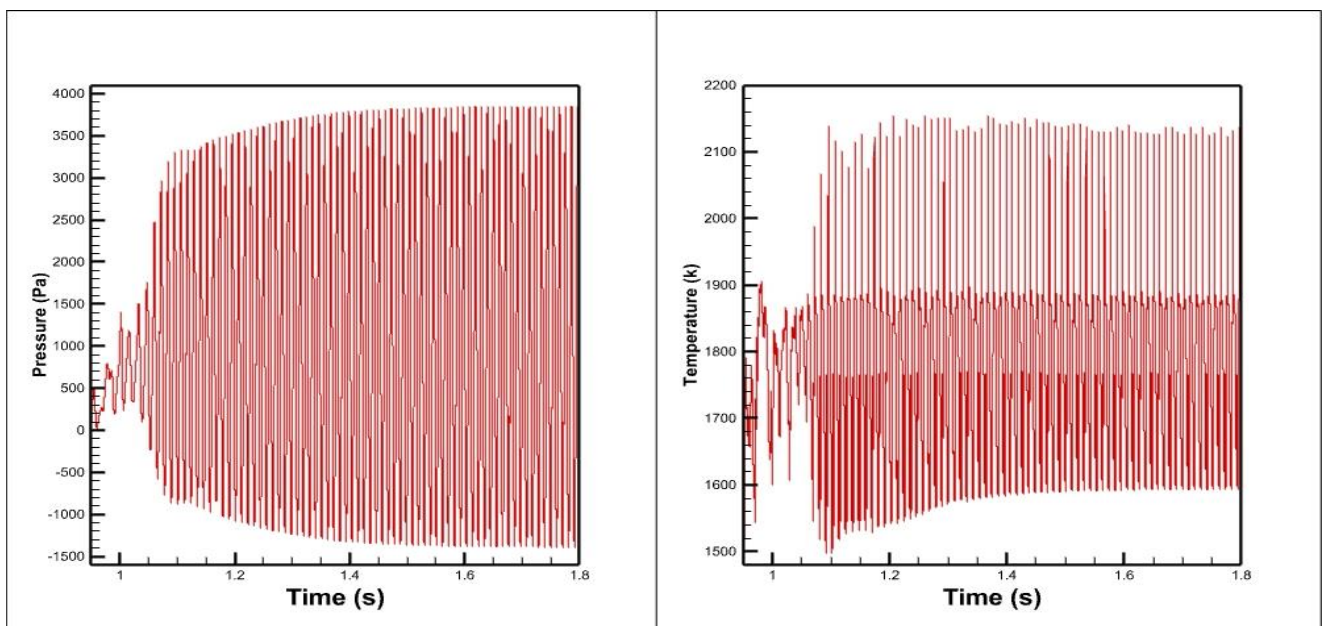

Figure 8. Limit cycle pressure and temperature within the combustion chamber.

From the CFD simulation model, we can find out that the heat release and pressure oscillation are in a phase relationship as seen in Figure 9, which demonstrates the temporal evolution of pressure oscillation with temperature. The heat release will drive pressure oscillation according to the Rayleigh criterion and reach the combustion instability condition for this case.

The produced pressure waves are sinusoidal, which split into compression and rarefaction waves. In compression, the wave gradually increases with time until combustion occurs at 1.017 s when the pressure rises above atmospheric value level, as indicated in reference [20] where the temperature curve steps up abruptly, meaning that combustion with re-ignition starts within the combustion chamber before propagating downstream.

The hot gas products are expelled due to the high pressure produced by combustion and then exit from the tailpipe into the atmosphere. Whereas, rarefaction waves result in introducing a new charge of fuel and air.

The numerical simulation was used to investigate the parameter values of the current model, which fluctuates throughout the given domain of pulse combustor with time during the continuous operation of the model
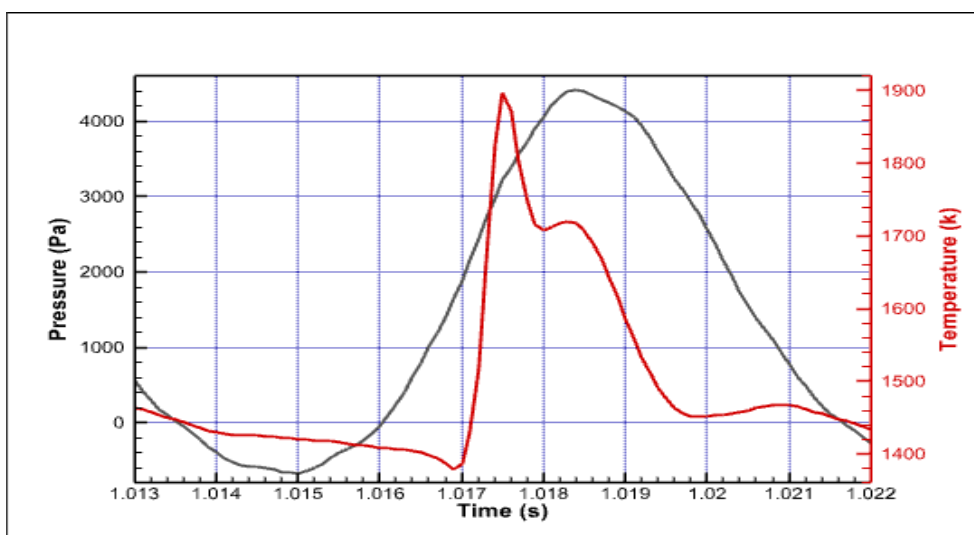

**Figure 9. Pressure and temperature variations of combustion instability
within the combustion chamber.**

The simulation of the current study was performed by using propane as a fuel. Figure 10, displays the relationship between temperature and propane mass fraction. This figure demonstrates the detailed process of combustion in pulsed combustion cycles and the direct relationship between temperature and fuel consumed in a pulse combustor. The mixture is heated from the inlet port by mixing with hot gases and the wall along with the location of propane consumption.

The re-ignition of combustion was signaled by a sharp decrease in the presence of the propane mass fraction from 0.32 to the minimum value consumed. The peak temperature of 1900 K is located at a stoichiometric mixture fraction. These begin in the mixture near the flame holder as seen in Figure 5, frame 1.0175 s. According to the method of fuel injection, some fuel from the rich flow is transported away from the flame and never burned in the absence of self-breathing oxygen, where it is entirely consumed by combustion in the combustion chamber.
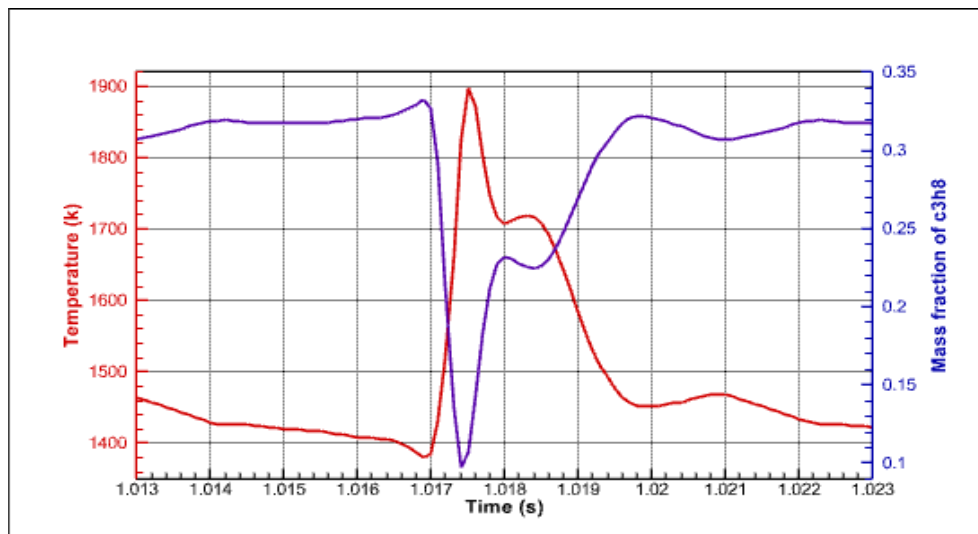
Figure 10. Temperature versus propane mass fraction variation within the combustion chamber.

The increasing rate of consumption of propane due to fuel bursts causes a corresponding increase in the rate of formation of CO_2 and CO, in response to the availability of air and fuel, followed by a decrease in response to the consumption of air and fuel at the end of combustion.

Figure 11 demonstrates the temperature variation in the combustion chamber as a function of CO_2 mass fraction. The variation of CO_2 formation is influenced by the fuel consumption and accompanied by heat generation release, so, CO_2 mass fraction curve resembles the temperature variation curve in the cycles of the combustor. The peak value of CO_2 has a mass fraction of 0.15 in the reaction zone, which is the maximum value at 1800 K as the maximum temperature, then drops near to 0.11 at the end of the combustion cycle at 1450 K, then a sudden rise at the start of the re-ignition and the beginning of combustion again. This curve is important because it emphasizes the close relationship between the temperature trend and mass fraction of carbon dioxide in pulse combustion.
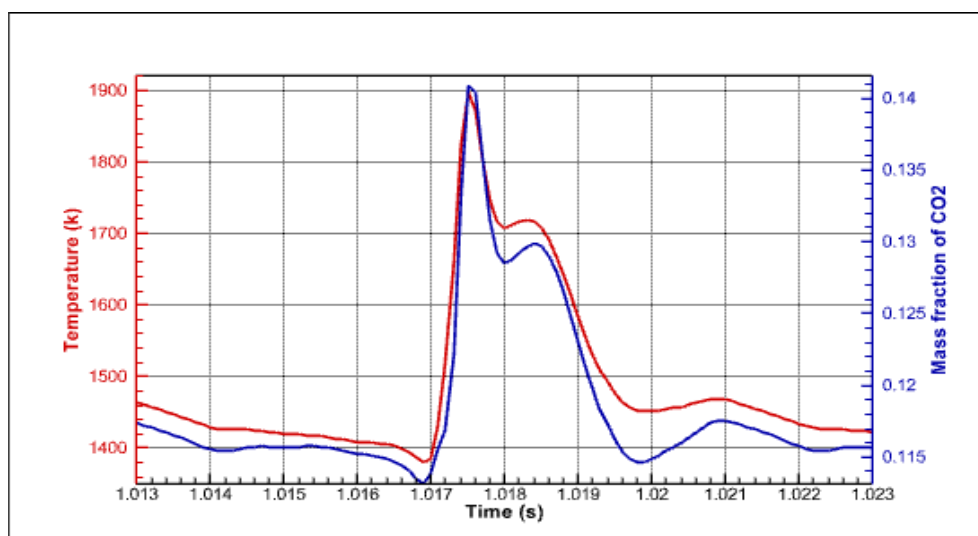

**Figure 11. The variation of temperature with the mass fraction of CO_2
within the combustion chamber.**

Figure 12 shows the temperature varied with the mass fraction of CO inside the combustion chamber. As shown in this figure, CO is used to scientifically demonstrate the re-ignition start, which begins to rise suddenly at the start of re-ignition to 0.016 mass fraction, then drops to 0.0055, its lowest value, before returning to the usual direction of flue gases downstream. Due to the high temperature and local availability of sufficient oxygen, CO is oxidized to CO_2 according to equation freeze CO mass fraction (9). This figure is significant for a deep understanding of the re-ignition start of pulse combustion and to reasonably predict final product emissions with combustion flame temperature.
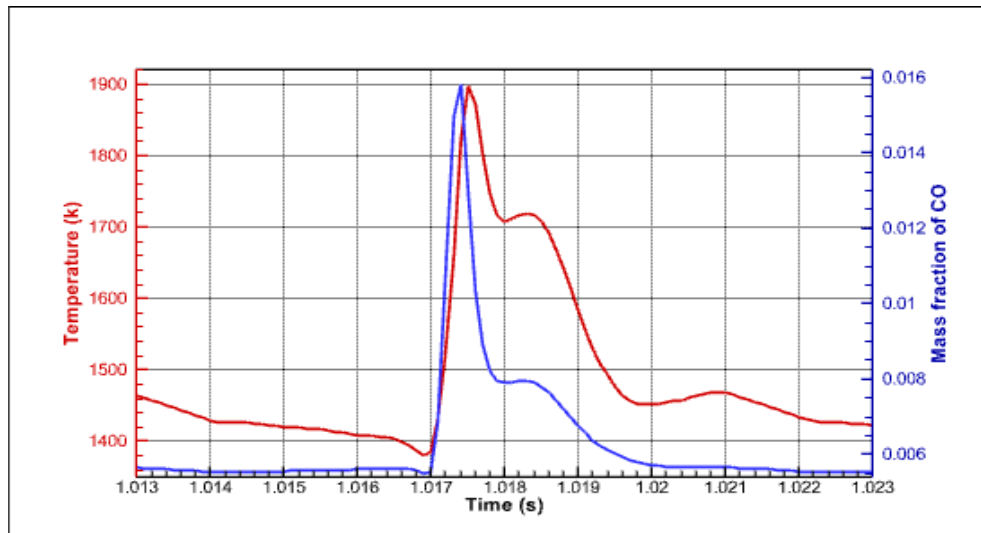

**Figure 12. Variation of temperature with the mass fraction of CO
within the combustion chamber.**

4.3. Model Validation

Successful experiments were conducted using combustor configurations that included a flame holder, as shown in Figure 3. The fuel flow rate of propane ranged between 0.18 and 0.2 g/s, which was the key measured parameter. To verify the model accuracy, the experimental results are accurately compared with the predicted model frequency and pressure amplitude. As shown in Figure 13, the measured experimental value of pressure amplitude at the sensor control point is 2950 Pa, while the model prediction is 3170 Pa. They are sufficiently in good agreement on the pressure amplitude. The numerical pressure simulation provided a better compatibility result with the typical oscillating pressure of the experimental signal to a satisfactory degree, regardless of the difference in pressure values. The pressure difference is attributed to the model's use of a two-step reaction mechanism for the EDM combustion model. In addition, the CFD simulation model does not take into account the friction losses within the combustion chamber and tailpipe.

The operating frequency of a pulse combustor or a pulsejet, f is determined from the following formula, as a function of the total length of the tailpipe and combustion chamber, and the speed of sound which is a function of the outlet temperature

$$f = \frac{C}{4l} \ (11)$$

Where:

 C: speed of sound, based on the outlet temperature, m/s, and
 L: length of combustion chamber and tailpipe, m.

The speed of sound is given by

$$C = \sqrt{\gamma RT}$$

Where:

γ: capacity heat ratio (adiabatic index, or specific heat ratio),
R: universal gas constant, J/kg K, and
T: outlet gas temperature, K.

For T = 770 K, and considering the gas to be air, then C= 557 m/s.

Thus, $f = \dfrac{557}{4*1.33} = 108$ Hz

The experimentally measured pressure wave frequency, for the present rig geometry, as indicated on the oscilloscope was 105 Hz. Thus, the pulse time is 11 ms. The calculated frequency from the above formula is 108 Hz, which is quite near to the measured value. The ANSYS- FLUENT model predicted a frequency of 112 Hz, as shown at the bottom of Figure 13 . It is in fairly good agreement with the measured frequency. This difference, which is not large, could be due to measurement accuracy. The frequency is calculated by the model via Fast Fourier Transform. It calculates Fourier Transformation for the variation in the pressure curve inside the apparatus, then the frequency and amplitude of the pressure wave.
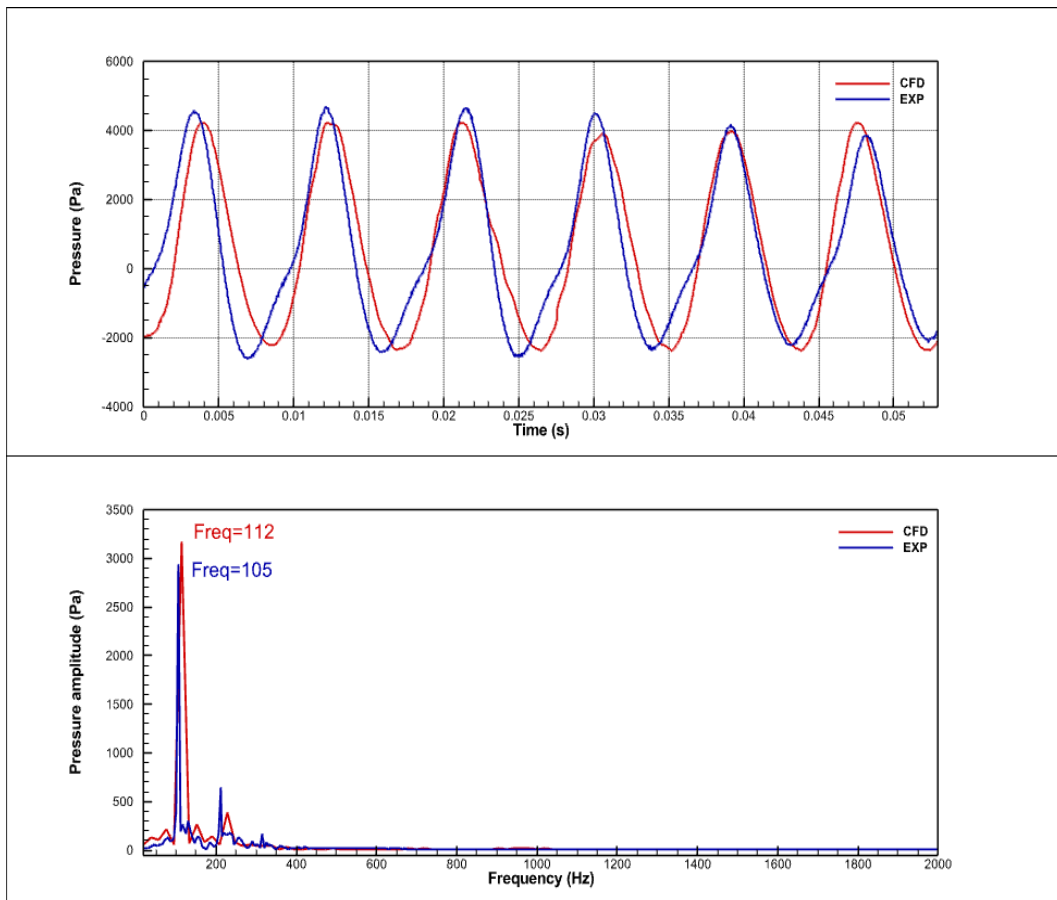

**Figure 13. Experimental and prediction pressure variation inside the combustion
chamber with frequency.**

5. CONCLUSIONS

A numerical simulation model was developed to analyze and study the combustion process in a valveless pulse combustor. A pulse combustor, equipped with measuring instruments, was designed and typically constructed. Model outputs were validated via comparison with experimental results, and fairly good agreement was found.

The main conclusions are:

● The combustion instability of the self-excited acoustic frequency mode in pulse combustion is accurately achieved by the predictions of the developed CFD model.

● The measured pressure wave frequency is 105 Hz, and the predicted model value is 112 Hz. The two specific frequencies are not far apart, with a 7% error, so a satisfactory agreement exists, which supports model validation.

● A significantly weak ignition takes place at the interface of the mixing layer between fuel and air flows near the entrance due to mixing with remaining hot gases from the previous cycle. It is quenched and does not continue, as there is insufficient energy to sustain its continuation. However, it contributes to raise the temperature of the mixture that burns later.

● Due to recirculation zones formed by swirling flows around the bluff-body, the flames stabilized and naturally extended in the vicinity of it. The flame propagates in the opposite direction to the fresh charge of fuel and air issuing from the inlet. That allows the flammable mixture of gases to re-ignite again within the mixing zone to continue the combustion. This was the major projected source of re-ignition.

● The re-ignition source is typically affected by the specified location of the flame-holder, which is useful for evaluating the performance of the pulse combustor.

● The high wall temperature aids in heating the mixture by radiation, without igniting it

● The phase relations between periodic variations of pressure, temperature, and mass fraction of propane stimulate the coupling between acoustic oscillations and the heat release rate according to the Rayleigh criterion.

● The progressive variation in the production of CO and CO_2 defines the flame extinction and re-ignition due to the change in oxygen and fuel consumption in the pulse combustor.

Declaration of conflict of interest

The authors declare that there is no conflict of interest in publishing this paper.

Nomenclature

Cp Specific heat (J/kgK).

D Diameter / geometrical characteristic length (m).

E Specific total energy.

e Internal energy.

F Fluid.

h Heat transfer coefficient (W/m^2 K).

K Thermal conductivity (W/MK).

k Turbulent kinetic energy (m^2/s^2).

P Pressure.

S Rate of the strain tensor.

T Temperature (K).

u Velocity.

U Average velocity (m/s).

x Axial position.

Y mass fraction.

Greek letters

μ Molecular viscosity (kg/ms).

δ Boundary layer thickness (m).

ε Turbulent energy dissipation rate (m^2/s^3).

ρ Density (kg/m^3).

τ_{ij} Stress tensor.

$\dot{\omega}$ Chemical production rate.

Subscripts

i, j, k Cartesian tensor indices or species indices.

Superscripts

s source.

REFERENCES

[1] Y. Kwon, B. Lee, Stability of the Rijke thermoacoustic oscillation, 78 (1985) 1414–1420.

[2] U.S. Department of Energy National Energy Technology, Pulse Combustor Design A DOE Assessment DOE/NETL-2003/1190, (2003) 1–44. www.netl.doe.gov.

[3] A.F. El-Sayed, Fundamentals of aircraft and rocket propulsion, 2016. https://doi.org/10.1007/978-1-4471-6796-9.

[4] G. Rogacki, C. Strumillo, P. Wawrzyniak, I. Zbicinski, Pulse combustion and supercritical fluid techniques as examples of innovative drying technologies, Dev. Chem. Eng. Miner. Process. 10 (2002) 415–428. https://doi.org/10.1002/apj.5500100412.

[5] T.R. Karthick, T.R.M. Aro, M.B.S. Shankar, M. Vinoth, Design and Optimization of Valveless Pulsejet Engine, 4 (2014) 56–59.

[6] V. Anand, J. Jodele, A. Zahn, A. Geller, E. Prisell, O. Lyrsell, E. Gutmark, Revisiting the Argus pulsejet engine of V-1 buzz bombs: An experimental investigation of the first mass-produced pressure gain combustion device, Exp. Therm. Fluid Sci. 109 (2019) 109910. https://doi.org/10.1016/j.expthermflusci.2019.109910.

[7] M.L. Coleman, Overview of Pulse Detonation Propulsion Technology, Chem. Propuls. Inf. Agency Columbia Md. (2001) 1–53. https://apps.dtic.mil/dtic/tr/fulltext/u2/a390257.pdf%0Ahttp://www.dtic.mil/dtic/tr/fulltext/u2/a390257.pdf.

[8] U. Sreekanth, B.S. Rao, A. Nagaraju, Performance and Analysis on Valveless Pulse Jet Engine, Imp. J. Interdiscip. Res. 3 (2017) 34–38.

[9] X. Meng, W. De Jong, T. Kudra, A state-of-the-art review of pulse combustion: Principles, modeling, applications and R&D issues, Renew. Sustain. Energy Rev. 55 (2016) 73–114. https://doi.org/10.1016/j.rser.2015.10.110.

[10] S. Modi, S. Khinchi, N. Rajpurohit, A. Rami, D. Sathish, Design and Development of Valveless Pulsejet Engine, in: 3rd Int. Conf. Energy, Power Environ. Towar. Clean Energy Technol. ICEPE 2020, Institute of Electrical and Electronics Engineers Inc., 2021: p. 6. https://doi.org/10.1109/ICEPE50861.2021.9404374.

[11] M. Zhai, L. Guo, Z. Wang, Y. Xu, Y. Zhang, P. Dong, Q. Li, Ignition process in a Helmholtz-type valveless self-excited pulse combustor, Exp. Therm. Fluid Sci. 88 (2017) 187–193. https://doi.org/10.1016/j.expthermflusci.2017.05.026.

[12] G. Benelli, G. De Michele, V. Cossalter, M. Da Lio, G. Rossi, Simulation of large non-linear thermo-acoustic vibrations in a pulsating combustor, Symp. Combust. 24 (1992) 1307–1313. https://doi.org/10.1016/S0082-0784(06)80152-9.

[13] K. Tajiri, S. Menon, LES of combustion dynamics in a pulse combustor, 39th Aerosp. Sci. Meet. Exhib. (2001). https://doi.org/10.2514/6.2001-194.

[14] Z. Xi, Z. Fu, X. Hu, S.W. Sabir, Y. Jiang, An investigation on flame shape and size for a high-pressure turbulent non-premixed swirl combustion, Energies. 11 (2018) 1–20. https://doi.org/10.3390/en11040930.

[15] W. Zhonghua, A.S. Mujumdar, Pulse combustion characteristics of various gaseous fuels, Energy and Fuels. 22 (2008) 915–924. https://doi.org/10.1021/ef7004207.

[16] Y. Xu, M. Zhai, L. Guo, P. Dong, J. Chen, Z. Wang, Characteristics of the pulsating flow and heat transfer in an elbow tailpipe of a self-excited Helmholtz pulse combustor, Appl. Therm.

Eng. 108 (2016) 567–580. https://doi.org/10.1016/j.applthermaleng.2016.07.114.

[17] Y. Xu, M. Zhai, P. Dong, F. Wang, Q. Zhu, Modeling of a self-excited pulse combustor and stability analysis, Combust. Theory Model. 15 (2011) 623–643. https://doi.org/10.1080/13647830.2011.556258.

[18] I. Ansys, ANSYS Fluent Meshing User ' s Guide,Release 15.0, ANSYS, Inc., Canonsburg, PA15317. 15317 (2013) 724–746.

[19] Q. Li, H. Yang, Y. Wang, P. Wang, Accuracy improvement of the modified EDM model for non-premixed turbulent combustion in gas turbine, Case Stud. Therm. Eng. 6 (2015) 69–76. https://doi.org/10.1016/j.csite.2015.07.002.

[20] I. Smajevic, Experimental study and computational modelling of gas fired pulse combustion, Int. J. Automot. Mech. Eng. 1 (2010) 1–12. https://doi.org/10.15282/ijame.1.2010.1.0001.